Anatomically shaped tissue-engineered cartilage with tunable and inducible anticytokine delivery for biological joint resurfacing

Franklin T. Moutos[a], Katherine A. Glass[b,c,d], Sarah A. Compton[a], Alison K. Ross[b,c], Charles A. Gersbach[d], Farshid Guilak[a,b,c,d,1,2], and Bradley T. Estes[a,1,2]

[a]Cytex Therapeutics, Durham, NC 27705; [b]Department of Orthopedic Surgery, Washington University, St. Louis, MO 63110; [c]Shriners Hospitals for Children, St. Louis, MO 63110; and [d]Department of Biomedical Engineering, Duke University, Durham, NC 27708

Edited by Shu Chien, University of California, San Diego, La Jolla, CA, and approved June 10, 2016 (received for review February 2, 2016)

Biological resurfacing of entire articular surfaces represents an important but challenging strategy for treatment of cartilage degeneration that occurs in osteoarthritis. Not only does this approach require anatomically sized and functional engineered cartilage, but the inflammatory environment within an arthritic joint may also inhibit chondrogenesis and induce degradation of native and engineered cartilage. The goal of this study was to use adult stem cells to engineer anatomically shaped, functional cartilage constructs capable of tunable and inducible expression of antiinflammatory molecules, specifically IL-1 receptor antagonist (IL-1Ra). Large (22-mm-diameter) hemispherical scaffolds were fabricated from 3D woven poly(ε-caprolactone) (PCL) fibers into two different configurations and seeded with human adipose-derived stem cells (ASCs). Doxycycline (dox)-inducible lentiviral vectors containing eGFP or IL-1Ra transgenes were immobilized to the PCL to transduce ASCs upon seeding, and constructs were cultured in chondrogenic conditions for 28 d. Constructs showed biomimetic cartilage properties and uniform tissue growth while maintaining their anatomic shape throughout culture. IL-1Ra–expressing constructs produced nearly 1 μg/mL of IL-1Ra upon controlled induction with dox. Treatment with IL-1 significantly increased matrix metalloprotease activity in the conditioned media of eGFP-expressing constructs but not in IL-1Ra–expressing constructs. Our findings show that advanced textile manufacturing combined with scaffold-mediated gene delivery can be used to tissue engineer large anatomically shaped cartilage constructs that possess controlled delivery of anticytokine therapy. Importantly, these cartilage constructs have the potential to provide mechanical functionality immediately upon implantation, as they will need to replace a majority, if not the entire joint surface to restore function.

tissue engineering | gene therapy | osteoarthritis | mesenchymal stem cell | cartilage repair

Under normal physiologic circumstances, articular cartilage functions for decades as a nearly frictionless surface in diarthrodial joints, while exposed to loads of several times body weight (reviewed in ref. 1). This remarkable mechanical function is attributed to the unique structure and composition of the cartilage ECM (2). In a healthy joint, the compressive, tensile, and viscoelastic properties of hyaline cartilage contribute to load bearing, energy dissipation, and joint lubrication over the lifetime of the joint. However, degeneration of the cartilage is associated with significant loss of cartilage function that contributes to further degeneration of the joint, which ultimately leads to osteoarthritis (OA), a debilitating disease affecting over 27 million people in the United States alone (3). For patients suffering from end-stage OA of the hip, the standard surgical treatment is total hip arthroplasty (THA), where the entire joint is removed and replaced by an artificial ball and socket. Whereas this procedure has proven effective in the aging population, only a low percentage of young, active patients opt for THA. This is attributed to shortened projected lifetime of a hip implant for an active patient and the subsequent need for revision surgery, which is associated with significant complications, comorbidities, overall decreased effectiveness, and less patient satisfaction (4–9). The ability to repair or regenerate cartilage using tissue-engineering strategies could have a tremendous impact on the treatment of OA for the growing population of active patients with hip OA. To this end, there has been a significant increase in research and development aimed at improving cartilage repair strategies, which include marrow stimulation, osteochondral transfer, and autologous chondrocyte implantation (ACI) (10). However, whereas current cartilage repair strategies have shown some clinical success in treating small, defined focal defects (~2–3 cm in diameter), they are insufficient to treat large cartilage lesions and have not been targeted as a treatment for end-stage OA.

An important challenge in the development of biological resurfacing techniques for treating OA is the ability to manufacture large engineered tissue constructs with patient-specific geometries that precisely match the native joint surface, while withstanding the harsh mechanical and biochemical environment of the damaged joint. Meeting these criteria would provide the ability to support a regenerative response for long-term restoration of joint function. Despite this, there have been several initial studies on cartilage joint resurfacing (11–14). Hung et al. (13) and Hung and colleagues (14) demonstrated proof of concept for joint

Significance

Whereas some success has been realized treating isolated, focal defects or lesions of articular cartilage, the complete resurfacing of synovial joints remains an important challenge for the treatment of osteoarthritis. Here, we develop an anatomically shaped, functional cartilage construct based on a 3D woven scaffold that can provide for total joint resurfacing, with capabilities for tunable and inducible production of anticytokine therapy to protect diseased or injured joints from pathologic inflammation. An important advance of this work is the incorporation of a technique for scaffold-mediated viral gene delivery for overexpression of antiinflammatory molecules within the joint. This approach provides a foundation for total biological cartilage resurfacing to treat end-stage osteoarthritis for young patients, who currently have few therapeutic options.

Author contributions: F.T.M., K.A.G., S.A.C., A.K.R., C.A.G., F.G., and B.T.E. designed research; F.T.M., K.A.G., S.A.C., A.K.R., and B.T.E. performed research; F.T.M., C.A.G., F.G., and B.T.E. contributed new reagents/analytic tools; F.T.M., K.A.G., S.A.C., A.K.R., and B.T.E. analyzed data; F.T.M., K.A.G., S.A.C., A.K.R., C.A.G., F.G., and B.T.E. wrote the paper.

Conflict of interest statement: F.T.M., F.G., and B.T.E. are paid employees of Cytex Therapeutics and have patent filings relevant to the technology in this study. S.A.C. is a past employee of Cytex Therapeutics.

This article is a PNAS Direct Submission.

Freely available online through the PNAS open access option.

[1]F.G. and B.T.E. contributed equally to this work.

[2]To whom correspondence may be addressed. Email: guilakf@wudosis.wustl.edu or bradley.estes@cytextherapeutics.com.

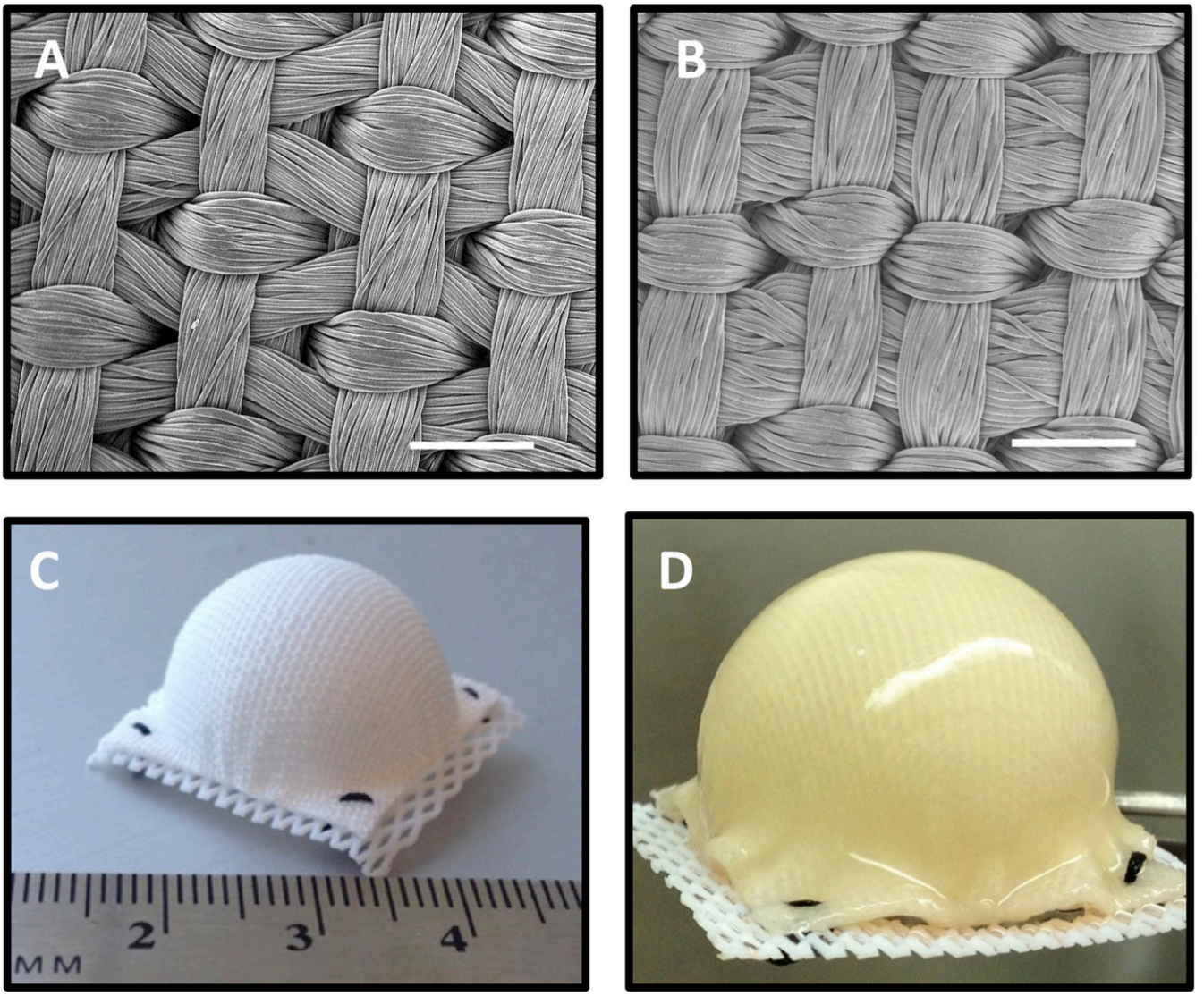

Fig. 1. (*A*) Surface SEM of scaffold variant 1 and (*B*) scaffold variant 2. (Scale bar, 0.5 mm.) (*C*) Hemispherical-shaped 3D woven PCL scaffold before seeding with human ASCs and (*D*) after 38 d of culture.

resurfacing using young bovine chondrocytes encapsulated in agarose cultured on bovine trabecular bone and later modeled nutrient and diffusion related parameters for growing large-scale constructs. More recently, in vivo studies in rabbits have used polymer 3D printed scaffolds in "anatomically correct" orthotopic models (11, 12). In these two studies, the authors present encouraging data on this resurfacing approach using bioprinted scaffolds, demonstrating that polymer-based, fully interconnected pore composites could act as a scaffold for cell attachment and cartilaginous tissue generation (11, 12). Although not as extensive as the resurfacing in the aforementioned publications, a scaffold-free construct has also been used successfully in a rabbit model for articular cartilage repair, in which autologous chondrocytes are expanded in vitro to form a neocartilage layer (15). In another study, Bhumiratana et al. (16) used condensed mesenchymal cell bodies that were fused together to grow centimeter-sized, anatomically shaped pieces of human articular cartilage over 5 wk of culture. However, none of these approaches provide biomimetic cartilage properties at the time of initial cell seeding, nor do they provide capabilities for long-term tunable drug delivery to the joint.

There is growing evidence indicating that proinflammatory cytokines, and particularly IL-1, play an important role in the pathogenesis of OA (17–19), as well as the inhibition of mesenchymal stem cell (MSC)-based repair of cartilage (20–25). However, natural inflammatory modulators such as IL-1 receptor antagonist (IL-1Ra) can inhibit IL-1 signaling (26), and studies have shown that biomaterial-mediated delivery of IL-1Ra can mitigate the degradative effects of IL-1 (27). A single intraarticular injection of recombinant IL-1Ra acutely following an anterior cruciate ligament (ACL) tear has been shown to improve joint function and decrease pain (28), but the recombinant protein has a short half-life within the joint. This strategy has not been as successful for primary OA treatment (29). IL-1Ra gene therapy, in which virus (30) or cells transduced ex vivo (31) are injected into the joint, has shown promise in animal models and has progressed to clinical trials, demonstrating the importance of IL-1 as a target in OA treatment and the potential of IL-1Ra as a therapeutic (reviewed in ref. 32). This approach can avoid repeated, systemic injection of expensive biologic drugs, but does not provide a functional replacement for severely damaged cartilage. We have previously

developed small cartilage constructs (5-mm disks) that are capable of inducible and tunable IL-1Ra production using scaffold-mediated lentiviral transduction of human MSCs (33). These IL-1Ra–expressing constructs were protected from IL-1 signaling, enabling them to develop robust engineered cartilage in an inflammatory environment in vitro.

The ultimate goal of this study was to engineer a functional tissue construct capable of resurfacing an entire osteoarthritic joint surface. To this end, we used an advanced weaving process to produce two variations of a 3D orthogonally woven textile scaffold (Fig. 1 *A* and *B*), each with different weaving patterns. These two similar, yet distinct structures had different overall porosities and were used to determine how weaving parameters can influence the mechanical and biochemical properties of the resulting engineered tissue. These variations were, in turn, used to develop large, anatomically shaped tissue-engineered constructs with the potential for resurfacing an entire diseased joint surface (Fig. 1 *C* and *D*). The basis of this approach is a hemispherical scaffold that can replicate the load-bearing mechanical properties of articular cartilage. In previous studies, we have shown that this 3D orthogonal structure displays many of the inhomogeneous, anisotropic, and viscoelastic mechanical properties of articular cartilage (34–36). The unique architecture was created using poly(ε-caprolactone) (PCL) fiber, a US Food and Drug Administration-approved biomaterial, which effectively provides an implant that not only recreates the physical and biomechanical properties of the native tissue, but also encourages cell infiltration, growth, and differentiation. In a second series of experiments, we combined this tissue engineering technology with a gene therapy approach for inducible and tunable antiinflammatory therapy to endow the engineered cartilage with the ability for exogenously controllable long-term anticytokine production. Scaffold-mediated gene delivery of a doxycycline (dox)-inducible lentiviral vector was used to transduce adipose-derived stem cells (ASCs) upon seeding to engineer cartilage constructs with tunable IL-1Ra overexpression. We characterized the ability of these IL-1Ra–expressing constructs to inhibit the effects of IL-1 on the development of in vitro engineered cartilage by analyzing histology, biochemical composition, and release of inflammatory factors.

Results

Gross Morphology, Histology, and Immunohistochemistry. All hemispherical constructs maintained their initial size and shape throughout the entire 38-d culture period with no indication of morphological distortion. By day 28, all constructs had developed a smooth and glistening gross appearance resulting from newly synthesized ECM that evenly covered both inner and outer surfaces of the scaffolds (Fig. 1*D* and Fig. 2). This uniform tissue distribution was further verified by confocal microscopy, which additionally showed cells and ECM filling the internal pores of the scaffolds (Fig. 2*B*) and covering the inner and outer surfaces (Fig. 2 *A* and *C*).

The ECM synthesized by the seeded ASCs appeared compositionally similar on both scaffold variants. Histological analysis revealed a highly cellular and collagenous matrix that stained positively for the presence of sulfated glycosaminoglycans (s-GAGs) (as stained by safranin-O) (Fig. 3). Furthermore, immunolabeling revealed positive staining for type II collagen, the primary collagen in articular cartilage ECM, and the chondroitin 4-sulfate epitope within all constructs (Fig. 3). Constructs also stained positive for low levels of collagen type I. Overall, the seeded

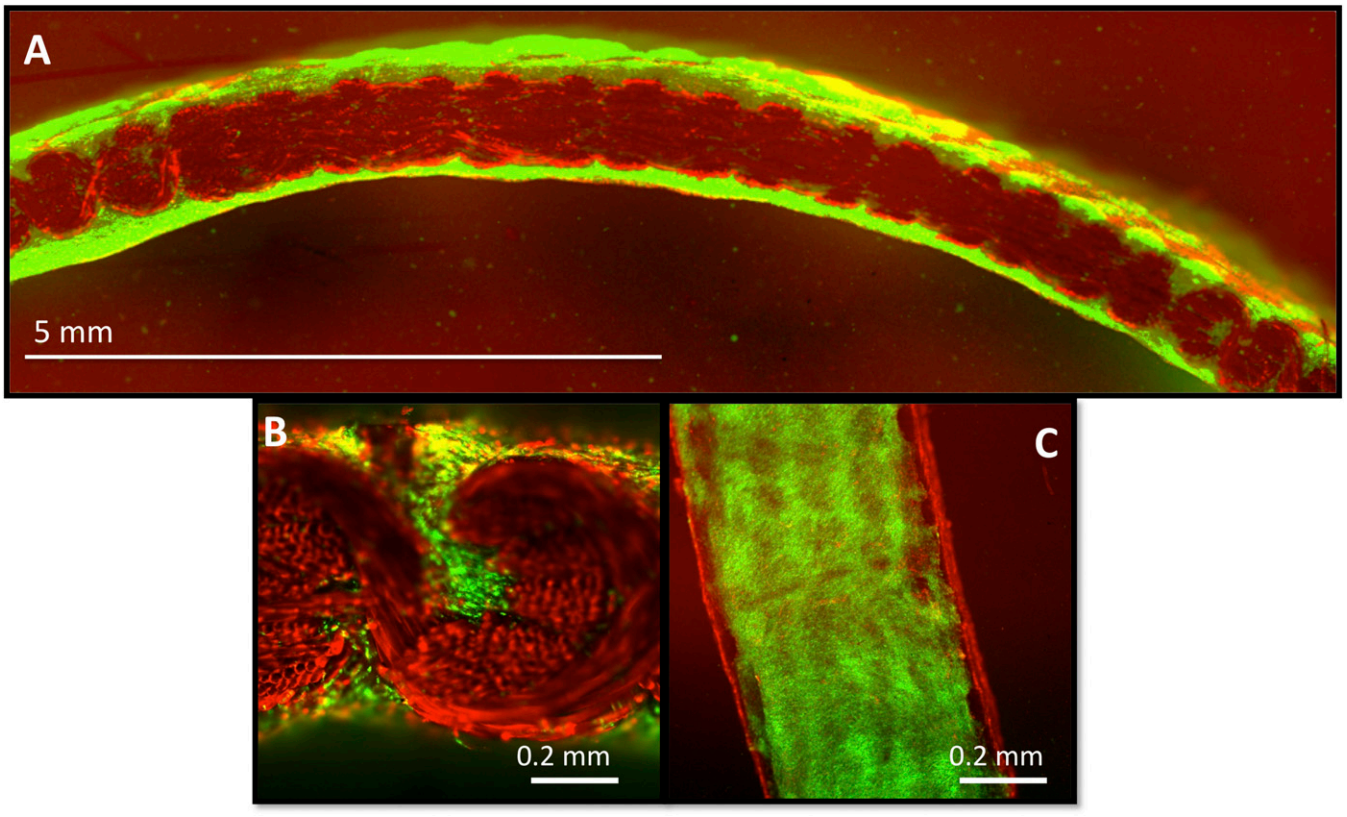

Fig. 2. (*A* and *B*) Cross-sectional confocal images at 38 d depicting live cells (green) embedded within an ECM and within the pores of the scaffold (red) fully covering the inner (*Bottom*) and outer (*Top*) layers of the hemisphere (variant 2). (*C*) Surface of a cut section of hemisphere demonstrates cell morphology and distribution over surface. Note the ethidium homodimer-1 dye is bound by the PCL fibers and therefore completely labels the synthetic scaffold red.

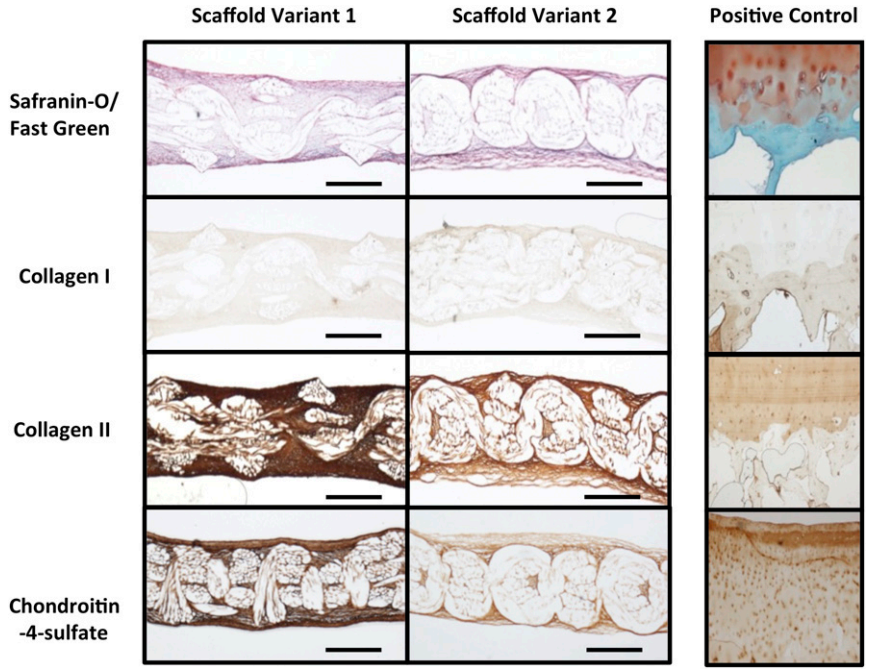

Fig. 3. Histology and IHC of hemispherical-shaped constructs at day 38 (cross-sectional views). Human osteochondral tissue (*Right* column) was used as a positive control for all staining protocols. (Scale bar, 0.5 mm.)

ASCs synthesized a uniform ECM that encapsulated both inner and outer surfaces of both scaffold variants and completely filled their internal pore spaces.

Biomechanical Analysis of Engineered Cartilage Hemispheres. Immediately after seeding (day 0), scaffold variant 1 displayed a compressive aggregate modulus (H_A) of 0.34 ± 0.02 MPa, whereas scaffold variant 2 displayed an H_A of 0.77 ± 0.09 MPa. By day 38, this initial value had increased by 90.0% to 0.66 ± 0.05 MPa for constructs based on scaffold variant 1 and by 38.9% to 1.07 ± 0.11 MPa for constructs based on scaffold variant 2 ($P < 0.05$, Fig. 4*A*). The apparent hydraulic permeability for both groups decreased by an order of magnitude from day 0 to day 38 ($P < 0.05$, Fig. 4*B*).

Measured by steady frictional shear, the equilibrium coefficient of friction (μ_{eq}) at day 0 was 0.13 ± 0.02 for scaffold variant 1, and 0.57 ± 0.10 for scaffold variant 2. Neither group showed statistically significantly changes over time; however, values trended toward one another as culture time increased. By day 38, μ_{eq} for constructs based on scaffold variant 1 had increased from initial values by ∼70% to 0.23 ± 0.01, whereas μ_{eq} for constructs based on scaffold variant 2 had decreased from initial values by ∼30% to 0.40 ± 0.05 (Fig. 4*C*).

Biochemical Analysis of Engineered Cartilage Hemispheres. DNA content increased significantly for both scaffold variants from day 0 to day 38, reaching a maximum level of 5.65 ± 0.4 μg per 5-mm sample for scaffold variant 1 and 4.91 ± 0.41 μg per 5-mm sample for scaffold variant 2 ($P < 0.05$, Fig. 5*B*). Significant increases over time were also observed with total collagen and total s-GAGs ($P < 0.05$, Fig. 5 *A* and *C*). By day 38, s-GAG content had increased 17-fold over initial values for scaffold variant 1, and 3-fold for scaffold variant 2. Similarly, collagen

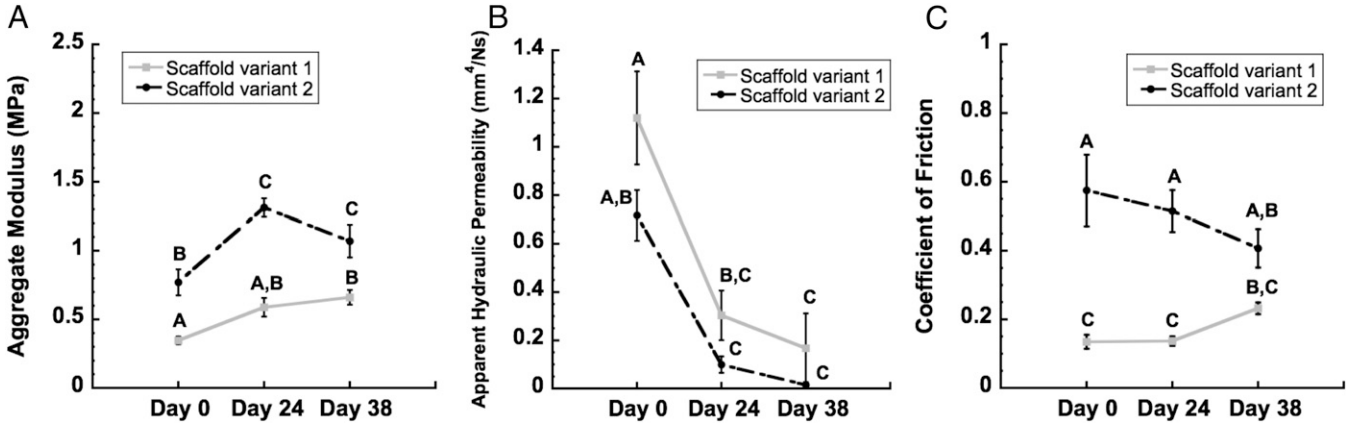

Fig. 4. Mechanical properties of constructs over total time in culture (i.e., expansion phase plus chondrogenesis phase). (*A*) Aggregate modulus and (*B*) apparent hydraulic permeability as determined by confined compression. (*C*) Equilibrium coefficient of friction as determined by steady shear. Groups not sharing the same letter are statistically different from each other (ANOVA, $P < 0.05$). Data are represented as mean ± SEM.

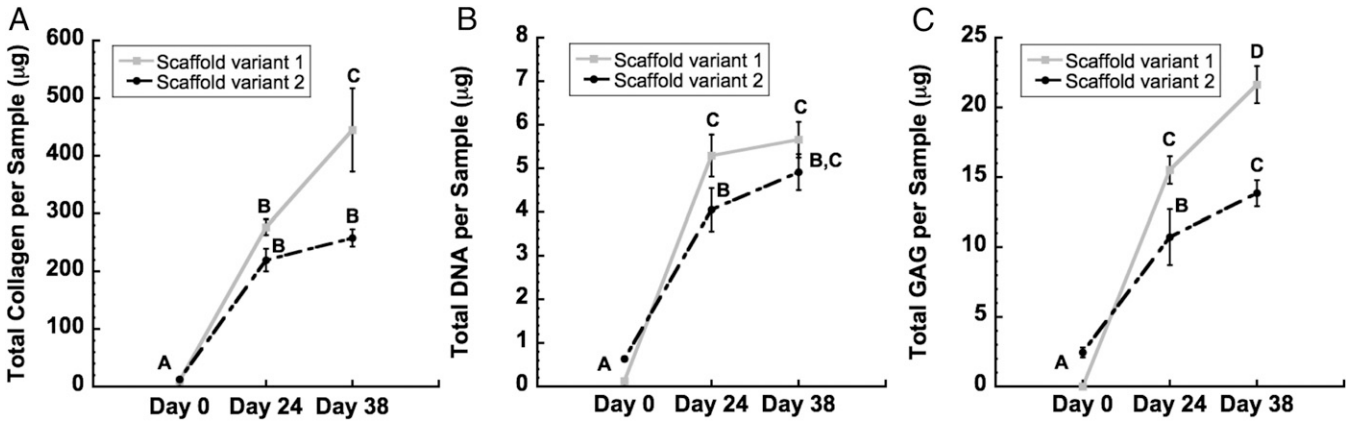

Fig. 5. Biochemical analysis of constructs over total time in culture (i.e., expansion phase plus chondrogenesis phase). (*A*) Total collagen, (*B*) total dsDNA, and (*C*) total s-GAG per 5-mm-diameter sample. Time points not sharing the same letter are statistically different from each other (ANOVA, $P < 0.05$). Data are represented as mean ± SEM.

content had increased 17-fold over baseline for scaffold variant 1 and 15-fold by day 38 for scaffold variant 2 (Fig. 5*A*).

Tunable IL-1Ra Production from Engineered Cartilage Hemispheres. Next, we combined this strategy for engineering functional cartilage hemispheres with scaffold-mediated lentiviral transduction to confer inducible anticytokine production from the tissue constructs. ASCs were isolated using enzymatic digestion from eGFP-expressing or nontransduced hemispheres after 14 d of culture in expansion medium with dox treatment (1 μg/mL). By flow cytometry, 70.8 ± 0.1% of these ASCs were $eGFP^+$, demonstrating efficient lentiviral transduction from these large anatomically shaped scaffolds.

After the addition of dox to the culture medium during chondrogenesis, high levels of IL-1Ra were measured in groups treated with and without IL-1. Peak levels of IL-1Ra were 1.08 ± 0.09 μg/mL on day 7, and there was no significant difference in IL-1Ra production from day 3 to day 28 (Fig. 6*B*). IL-1Ra production was not affected by IL-1 treatment. IL-1Ra concentrations averaged 2.6 ng/mL in the absence of dox at day 0 of chondrogenesis (Fig. 6*B*), demonstrating tight control and significant induction of IL-1Ra with the dox-inducible system.

Consistent with our previous study (33), there was an increase in total DNA, s-GAG, and collagen content over time in culture (Fig. 7 *A*–*C*). Unexpectedly, the s-GAG and collagen contents were not affected by IL-1 treatment in the eGFP-expressing or IL-1Ra–expressing constructs. However, total specific MMP activity in the conditioned medium of the eGFP-expressing hemispheres treated with IL-1 was significantly higher (over twofold) compared with all other groups at day 28 (Fig. 7*D*).

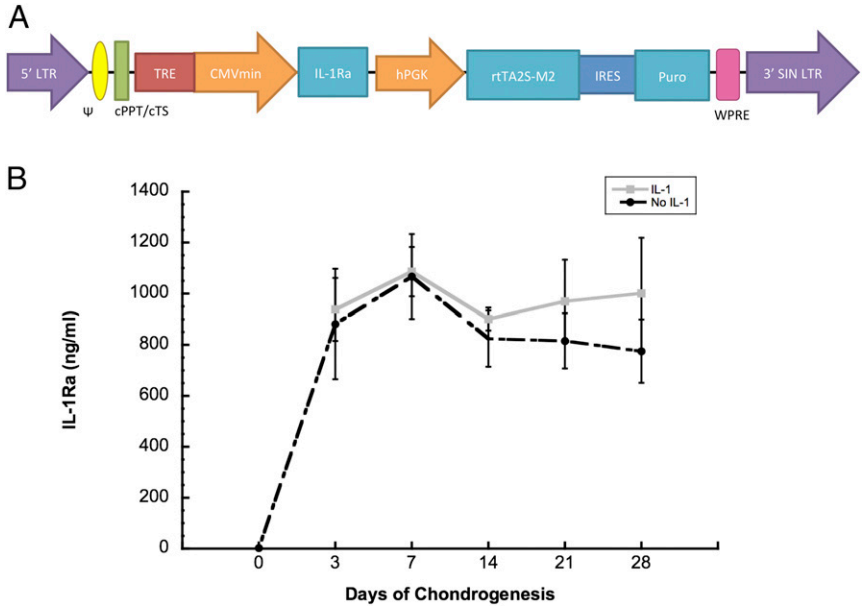

Fig. 6. (*A*) Schematic of dox-inducible lentiviral vector. IL-1Ra is driven by the tetracycline-regulated minimal CMV promoter (TRE-CMVmin). The human phosphoglycerate kinase (hPGK) promoter constitutively drives expression of the tet-responsive transactivator (rtTA2S-M2) and then, following an internal ribosomal entry site (IRES), the puromycin resistance gene (puro). The expression cassette is flanked by the 5′ and 3′ long-terminal repeats (LTR), psi packaging signal (ψ), the central polypurine tract (cPPT), central termination sequence (cTS), and the woodchuck hepatitis virus posttranscriptional regulatory element (WPRE). (*B*) IL-1Ra secretion for 48 h into culture media after 28 d of chondrogenesis either with or without IL-1 treatment. Day 0 shows the baseline expression before dox treatment.

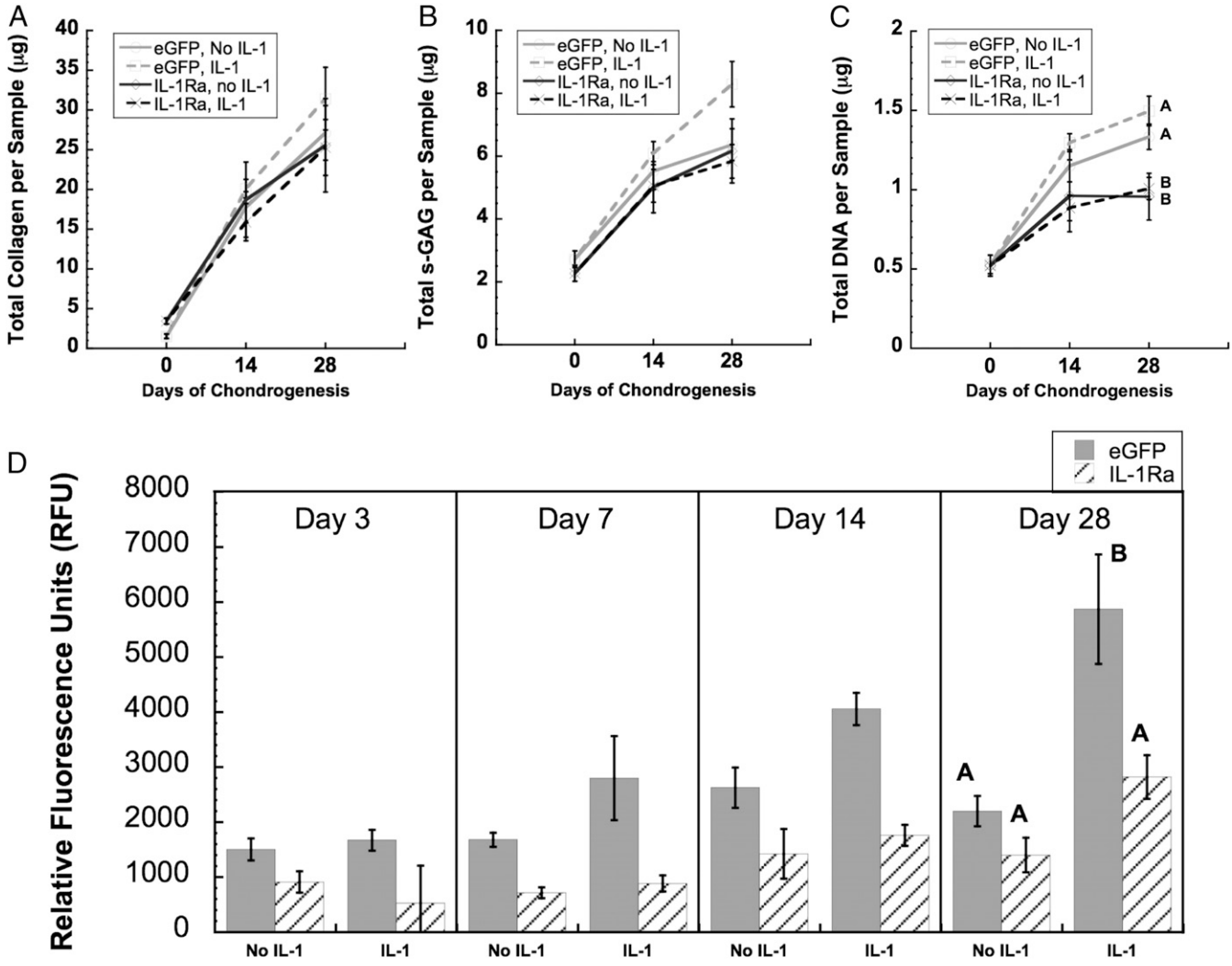

Fig. 7. (*A*) Total collagen per 5-mm-diameter sample, (*B*) total s-GAG per 5-mm-diameter sample, and (*C*) total DNA per 5-mm sample. (*D*) Total specific activity of MMPs released from cartilage constructs with or without IL-1, measured in culture media over 48 h at day 3, day 7, day 14, or day 28 of chondrogenesis. At day 28, groups with different letters are significantly different ($P < 0.05$) by ANOVA and Fisher's least significant difference post hoc (mean ± SEM, $n = 3$). At the other time points, there was no significant interaction term by ANOVA. At day 14, there were main effects of media and vector. At day 7, there was a main effect of vector.

Discussion

Our findings show that advanced 3D textile manufacturing combined with gene therapy can be used to tissue engineer large anatomically shaped cartilage constructs that possess controlled long-term anticytokine production capabilities. Importantly, these engineered cartilage constructs must provide mechanical functionality immediately upon implantation, as they will need to replace a majority, if not the entire joint surface to restore normal function. Using a technique for scaffold-mediated lentiviral transduction, ASCs within the scaffold were genetically modified to produce high levels of an anticytokine therapy (IL-1Ra) in an exogenously tunable and inducible manner. The combination of these technologies within one scaffold provides a foundation for the development of a tissue-engineering strategy for total joint resurfacing as a therapy for end-stage OA or other joint diseases, particularly for younger patients who have limited treatment options. Whereas a tissue engineering approach was used in the current study, alternative applications of this technology in vivo may involve the implantation of an acellular scaffold, which, if implanted in conjunction with current bone marrow stimulation techniques (e.g., microfracture), could facilitate endogenous stem cell infiltration and subsequent cell transduction in situ without the need for costly and time-consuming ex vivo culture.

A key finding of this study was the successful formation of scaffolds into hemispherical shapes that mimic native hip joint surfaces, while maintaining this anatomical shape throughout in vitro tissue development with no morphological distortion (Fig. 1*D*). This characteristic is based on the unique combination of the 3D orthogonally woven structure that provides initial flexibility, without folding or buckling, coupled with the strength and stiffness of the thermoplastic PCL yarn, all while maintaining regular, repeating pore structure for cell seeding and homogenous tissue synthesis (34, 35, 37). The molded hemispherical scaffolds displayed excellent dimensional stability over time, and, thus, the scaffolds were able to resist the cell-mediated contractile forces generated by the developing tissue.

We also demonstrated the ability to modulate the functional mechanical properties of our engineered hemispheres by controlling weave architecture. As expected, compression testing in this study revealed higher aggregate modulus values for scaffold variant 2 at all time points, which results from its tighter weave architecture and increased friction between constituent yarns

(Fig. 4*A*). The increase in modulus over time, seen in constructs with both scaffold variants, has been demonstrated in our previous work and occurs as ECM is deposited onto the scaffold, effectively binding its fibers and stiffening the entire construct (37, 38). Accumulating ECM, which fills the pores of the scaffolds and limits fluid flow, is also responsible for the decrease in apparent hydraulic permeability over time to values in the range of articular cartilage (39) (Fig. 4*B*). The coefficients of friction for both scaffold variants were also affected by the accumulation of tissue. At day 0, scaffold variant 1 displayed a significantly lower coefficient of friction due to its more loosely woven architecture, which presents fewer superficial *z* yarns or "high points" available for interaction with an opposing surface. As ECM was increasingly deposited over time, the inherent scaffold surface roughness was smoothed over and the coefficients of friction for the two constructs became more similar. By day 38, the difference was insignificant as the interface now consisted entirely of new ECM, which was compositionally the same on both scaffolds. Furthermore, these constructs displayed equilibrium coefficients of friction that were similar to those of native cartilage, as well as other engineered cartilage constructs, by day 38 (40–45).

In accordance with previous studies demonstrating the chondrogenic potential of ASCs (46–48), the ECM produced by ASCs seeded within the large PCL hemispheres stained positively for cartilage-specific macromolecules, which accumulated on all scaffolds over time (Fig. 3). At the end of the 38-d culture period, however, significantly higher amounts of total collagen and s-GAGs were present on scaffold variant 1 compared with scaffold variant 2 (Fig. 5). These data indicate that a relatively small increase in porosity (7.1% in the current study) can have profound effects on the ability of ECM components to be synthesized within the pore structure. It is important to note that the increase in pore size leading to this increased accumulation of cartilage ECM proteins has to be ultimately balanced by maintaining enough solid fiber volume fraction to support joint function when implanted in the joint. Our previous findings examining the changes in construct mechanical properties over time suggest that the specific tissue composition does not play as important a functional role in the context of this scaffold and tissue-engineering approach as it does with native tissue, because the bulk material properties of the biosynthetic composite should dictate performance of the implant (49).

In previous studies, agarose seeded with bovine chondrocytes was molded to create anatomically shaped retropatellar and trapeziometacarpal cartilage constructs (13). After 35 d in culture, significant GAG staining was noted, consistent with articular cartilage, but even 35 d were insufficient to obtain functional mechanical properties for the cartilage construct. This long-term culture and the inability to synthesize a functional matrix starting with a relatively weak hydrogel alludes to the need for a different strategy and perhaps the need for material reinforcement to meet the functional demands of the joint. Using 3D-printed PCL and custom machining, Lee et al. (12) demonstrated proof of concept for resurfacing a rabbit synovial joint in vivo and demonstrated that such an acellular scaffold infused with TGF-β3 can induce some cartilage regeneration within the joint space. The use of a cell-based woven PCL scaffold may confer some advantage due to the ability to replace only the affected cartilage layer while preserving valuable bone stock for future intervention, as well as the ability to easily conform the woven implant to complex surface geometries without custom printing and/or machining. Furthermore, the approach in the current study provides the capability for controlled drug delivery to the joint using a scaffold-mediated gene therapy technique.

An important advance of this work was the incorporation of a gene therapy approach that allows scaffold-mediated transduction of ASCs with lentivirus in situ, which could allow exogenous control of production of therapeutics locally within the joint in a tunable and inducible manner. Previous scaffold-mediated gene delivery approaches include release of encapsulated vectors from within a biomaterial as it degrades (50, 51) or immobilization on the scaffold surface to spatially control transduction (52, 53). However, these strategies have primarily generated transient gene expression by delivering plasmid DNA (50, 51) or nonintegrating viral vectors (52, 54). Lentiviral transduction causes integration of the expression cassette into the host cell genome, which remains for the lifetime of the target cell and its progeny. Additionally, previous strategies have not incorporated regulated gene expression systems. The dox-inducible expression cassette used in this study allows temporal control as well as a dynamic range of IL-1Ra secretion greater than two orders of magnitude (33, 55). Although we used this well-described dox-inducible system for the current study, other inducible systems could be used with this same overall strategy if the modulation of anticytokine therapy is indeed beneficial during tissue regeneration.

The engineered cartilage hemispheres in this study synthesized IL-1Ra at concentrations of 1 μg/mL in vitro, which should fully inhibit pathophysiologic levels of IL-1 found in OA joints (56). These levels of IL-1Ra secretion within the engineered cartilage hemispheres prevented the increase of MMP production induced by IL-1 in IL-1Ra–expressing constructs compared with eGFP-expressing constructs. Interestingly, unlike in human MSCs, IL-1 did not significantly inhibit s-GAG or collagen accumulation in human ASCs. This finding is consistent with previous data showing their relatively low catabolic response to IL-1 (57) compared with MSCs (38). In this regard, ASCs may provide certain advantages as a cell source, as their response will be less sensitive to the inflammatory environment of the joint while still maintaining a high sensitivity to exogenous control of transgene expression with dox. The ability to tune IL-1Ra overexpression is important in cases where inflammation may play an important physiologic role, such as during fracture healing (58). Furthermore, although IL-1Ra was used in this study, a similar approach may be readily used to deliver other antiinflammatory or proanabolic cytokines or growth factors (59). We did, however, observe lower DNA content throughout culture in the second part of our study, which may have been a result of cell transduction. If lentiviral transduction of ASCs does indeed affect cell proliferation as observed in this study, then multiplicity of infection could potentially be optimized (i.e., minimized) in an attempt to maximize tissue synthesis while maintaining sufficient overexpression of IL-1Ra for inflammation resistance.

An important design parameter for this scaffold was the use of a biomaterial that was resorbable but could also function for prolonged time in the joint while cells synthesize and assemble a functional matrix. Our results demonstrate that the 3D woven scaffolds exhibit an inverse correlation between mechanical properties and void fraction. Therefore, optimizing the scaffold geometry to have minimum, yet fully functional, mechanical properties with maximum void volume could provide for maximal tissue deposition and mechanical maturation of the ECM before the start of significant scaffold resorption. Whereas use of a resorbable material confers a theoretical advantage for in vivo use of ultimately only having native tissues in the repaired cartilage, an unknown factor in this system is the long-term time frame for PCL degradation and the resulting interaction of the scaffold with de novo tissue. Future studies will be required to examine this question in an orthotopic, in vivo study.

In summary, we have shown the development of large, anatomically shaped engineered cartilage hemispheres capable of tunable and inducible anticytokine production with functional properties matching articular cartilage. The anticytokine therapy was effective in preventing MMP production from the engineered cartilage, and it may have beneficial effects throughout

the repaired joint as well. The biomimetic scaffold was produced by 3D weaving PCL fibers into a porous structure that recreates the physical and biomechanical properties of the native tissue while encouraging cell infiltration, growth, and differentiation. The ability to accurately maintain initial size and anatomic shape, from manufacture of the scaffold to implantation of the tissue-engineered cartilage construct, will prove critical to the success of our custom-fit resurfacing approach. Additional in vivo studies are needed to elucidate the structural requirements, the need for proanabolic cytokine delivery, and the potential need to regulate the inflammation within the joint. This system shows promise as an inflammation-resistant engineered cartilage tissue for applications in whole joint resurfacing of injured and osteoarthritic hip joints.

Materials and Methods

Scaffold Production. Multifilament PCL yarns (EMS-Griltech) measuring ~150 μm in diameter were woven in three orthogonal directions (*x*, *y*, and *z* directions) to form 3D textile scaffolds (35, 49). While keeping overall thickness constant (~0.75 mm), two variations of this material (scaffold variant 1 and scaffold variant 2) were produced to demonstrate how physical and mechanical properties of the scaffold can be tuned by altering the relative spacing and positioning of the constituent yarns in the principal directions. Specifically, scaffold variant 1 was constructed with 15 *y*-direction yarns per centimeter, while scaffold variant 2 was constructed with 18 *y*-direction yarns per centimeter. Furthermore, yarns oriented in the *x* direction of scaffold variant 1 were separated by one *z*-direction yarn. This pattern (*x* yarn, *z* yarn, *x* yarn, *z* yarn) was repeated across the entire width of the scaffold (Fig. 1*A*). For scaffold variant 2, this repeat pattern was changed to: *x* yarn, *x* yarn, *z* yarn, *z* yarn (Fig. 1*B*). These variations in weaving parameters resulted in overall porosities of 52.5% for scaffold variant 1 and 45.4% for scaffold variant 2.

After weaving, the PCL scaffolds were immersed in a 4M NaOH bath for 15–16 h to clean the fibers and increase their surface hydrophilicity (60, 61). Scaffolds were then formed into 22-mm-diameter hemispherical shapes by enclosing the flat material in a custom-made aluminum mold and placing the mold into a 65 °C oven for 50 min. The thermoformed hemispherical-shaped scaffolds (~760 mm^2) were then demolded, sutured onto flat nylon mesh (Fig. 1*C*), placed into custom-made glass jar bioreactors, and sterilized using ethylene oxide gas. Three samples ($n = 3$) of each scaffold variant were produced for this study.

Construct Culture. Human ASCs from seven deidentified donors (female, nonsmoking, nondiabetic, ages 27–51, and body mass index of 22.5–28.2) were isolated from liposuction waste (Zen-Bio) and pooled into a superlot for use in this study. Because all tissues were harvested from deidentified donors, cells used in these studies were institutional review board exempt. The cells were plated on 225-cm^2 culture flasks (Corning) at an initial density of 8,000 cells per square centimeter and cultured at 37 °C at 5% CO_2 in expansion medium consisting of DMEM/F12 (Cambrex Bio Science), 10% (vol/vol) (lot selected) FBS (Atlas Biologicals), 1% penicillin–streptomyci–fungizone (Gibco), 5 ng/mL EGF (Roche Diagnostics), and 1 ng/mL bFGF (Roche Diagnostics). Expansion medium was replaced every 2–3 d as needed until cells became 90% confluent, at which time they were passaged and replated. Once cells reached passage 4, they were resuspended in expansion media and directly seeded onto the outer surface of the hemispherical-shaped scaffolds using a pipette (6 million cells per scaffold). Subsequently, the constructs were placed in a humidified incubator at 37 °C and 5% CO_2 for 60 min to allow cell attachment before adding 40 mL of expansion medium to each jar bioreactor. Constructs were maintained in expansion medium for 10 d to allow cells to proliferate throughout the scaffold and evenly cover all surfaces. On day 10 of culture, expansion medium was completely replaced with chondrogenic medium consisting of DMEM-high glucose (Gibco), 10% (vol/vol) FBS (Atlas Biologicals), 37.5 μg/mL ascorbic-2-phosphate (Sigma), 1% ITS+ premix (Collaborative Biomedical, Becton-Dickinson), 1% penicillin–streptomycin (Gibco), 100 nM dexamethasone (Sigma), 10 ng/mL TGF-β3 (R&D Systems), and 10 ng/mL BMP-6 (R&D Systems). Chondrogenic culture conditions were maintained for an additional 28 d after the initial 10-d expansion phase. For the duration of culture (i.e., both expansion phase and chondrogenic phase), one-half media changes were performed every 2–3 d. Furthermore, jar bioreactors were agitated at 60 rpm on an orbital shaker within the incubator to facilitate nutrient diffusion.

At days 0, 24, and 38, three 5-mm samples were harvested from each hemispherical-shaped construct along a radial path using a sterile biopsy punch. Samples were pooled for mechanical and biochemical analysis based on scaffold variant, resulting in nine samples per group per time point.

Lentivirus Production. Dox-inducible, lentiviral vectors containing the transgenes for IL-1Ra or eGFP were cloned previously (33). The dox-inducible lentivector (TMPrtTA, kindly provided by Olivier Danos, INSERM, Paris) is a "tet-on" system within one vector, which includes the rtTA2S-M2 reverse tetracycline-controlled transcriptional activator constitutively expressed from a human phosphoglycerate kinase promoter (Fig. 6*A*) (55). HEK293T/17 cells [American Type Culture Collection (ATCC); CRL-11268] were cotransfected with the transfer vector, packaging plasmid (psPAX2), and envelope plasmid (pMD2.G) through calcium phosphate precipitation to produce VSV-G–pseudotyped lentivirus as previously described (62). Lentivirus was concentrated ~80-fold using 100-kDa molecular weight cut-off filters (Millipore) and frozen at −80 °C. The functional titer of the lentivirus was determined via titration of eGFP lentivirus and transduction of HeLa cells (ATCC; CCL-2) using the Accuri flow cytometer (BD Biosciences) as previously described (62).

Scaffold-Mediated Transduction of ASCs in 3D Woven PCL Hemispheres. To modify the engineered cartilage hemispheres to express therapeutic cytokines, lentiviral vectors containing a transgene for IL-1Ra or eGFP were delivered to the ASCs via scaffold-mediated transduction ($n = 6$ per group). We used scaffold variant 2 for this set of experiments because its initial mechanical properties more closely resembled those of native cartilage of the femoral head (39). For scaffold-mediated transduction, PCL hemispheres were coated in 0.002% poly-L-lysine (PLL) (Sigma-Aldrich) overnight. PLL is a cationic polymer that helps immobilize negatively charged viral vectors to the PCL scaffold (53, 59, 63). Hemispheres were then rinsed in PBS (Gibco) and 200 μL of concentrated lentivirus containing an inducible expression cassette for IL-1Ra, or eGFP was added at a final biological titer of 6×10^6 transducing units per milliliter to each hemisphere. After an incubation at 37 °C and 5% CO_2, hemispheres were seeded with 6×10^6 cells per hemisphere and cultured in jar bioreactors. The hemispheres were cultured in expansion medium for 10 d to allow for cell attachment and proliferation. After this initial incubation period, constructs were further cultured for 28 d in chondrogenic medium with dox at 1 μg/mL. Beginning 3 d following chondrogenic induction, constructs were treated with either 0 or 100 pg/mL of recombinant human (rh)IL-1α, a pathophysiologic concentration found in the OA joint (56) ($n = 3$ per group). One-half medium changes were performed every 2–3 d and 2 mL of medium from each scaffold was collected and frozen at −20 °C at various time points to measure secretion of IL-1Ra and inflammatory mediators. Biopsy punches were taken at various time points as described to measure properties in the tissue longitudinally.

Histology and Immunohistochemistry. The 5-mm-diameter specimens were fixed in 10% (vol/vol) neutral buffered formalin overnight at 4 °C. After fixation, specimens were dehydrated in graded ethanol steps, cleared in xylene, and embedded in paraffin wax under vacuum. Embedded paraffin blocks were cut into 10-μm-thick sections using a Reichert–Jung microtome and mounted on SuperFrost microscope slides (Microm International). Samples were stained for s-GAGs and collagenous matrix using a 0.1% aqueous safranin-O solution and a 0.02% fast green solution, respectively, while also using hematoxylin as a nucleus counterstain. Human osteochondral tissue was used as a positive control. For immunohistochemical analysis (IHC), pepsin digestion of the sections to be labeled for types I and II collagen was performed using Digest-All (Life Technologies), and those sections to be stained for chondroitin 4-sulfate were digested with trypsin, followed by a soybean trypsin inhibitor, and finally with chondroitinase (all from Sigma). Monoclonal antibodies were used to identify type I collagen (ab6308; Abcam), type II collagen (II-II6B3; Developmental Studies Hybridoma Bank, University of Iowa, Iowa City, IA), and chondroitin 4-sulfate (2B6; AMSBIO). Human osteochondral samples were used as positive controls, and negative controls were prepared to rule out nonspecific labeling by omitting the primary antibody incubation step.

Biomechanical Analysis. Confined compression tests were performed on 3-mm-diameter cylindrical test specimens, cored from the centers of the harvested constructs with a biopsy punch, using an ELF 3200 series materials testing system (Bose). Specimens were placed in a 3-mm-diameter confining chamber in a bath filled with PBS, and a compressive load was applied using a solid piston against a rigid porous platen (porosity of 50%, pore size of 50–100 μm). Following equilibration of a 10 gram-force (gf) tare load, a step compressive load of 30 gf was applied to the sample and allowed to equilibrate for 2,000 s. Aggregate modulus (H_A) and apparent hydraulic permeability (k) were determined

numerically by matching the solution for axial strain to the experimental data for all creep tests using a three-parameter, nonlinear least-squares regression procedure assuming intrinsic incompressibility of the tissue (64, 65).

The equilibrium friction coefficient, μ_{eq}, was determined using a previously described shear friction testing method (45). Before the start of the test, samples were fixed using cyanoacrylate glue to an impermeable bottom platen in a PBS bath on an Ares AR-G2 rheometer (TA Instruments) and subjected to a 10% compressive tare strain using a stainless steel top platen. Once the imparted stress reached an equilibrium level (~1,800 s), an angular velocity of 10 rad/s was applied through the bottom platen for the duration of 120 s. Normal force, N, and frictional torque, T, were recorded and used for calculation of the equilibrium friction coefficient given by $\mu_{eq} = F/N$. By assuming that the distribution of unknown frictional shear is zero at the center and varies linearly along the radial direction of the cylindrical test specimen, the average frictional force, F, is given by $F = 4T/3r_0$, where r_0 is the radius of the specimen.

Biochemical Analysis. After mechanical testing, constructs were completely dried and weighed. Constructs were then diced and digested in papain for 12 h at 58 °C. DNA was measured using the Quant-iT PicoGreen Double-Strand DNA (dsDNA) assay (Life Technologies). S-GAG was measured using the dimethyl–methylene blue assay using chondroitin 4-sulfate as a standard and reading the optical density on a plate reader at 595 nm. Hydroxyproline (OHP) was used to determine total collagen content. Briefly, sample digest was acid hydrolyzed and reacted with *p*-dimethylaminobenzaldehyde and chloramine-T to measure OHP content per construct. Total collagen was then determined using 0.134 as the ratio of OHP to collagen (66).

Culture Medium Analyses. IL-1Ra secretion into the culture medium was measured with a human IL-1Ra ELISA (R&D Systems; DY280) following the manufacturer's protocol, with the color detected at 450 nm with a correction at 540 nm. All samples were run in duplicate. Total specific MMP activity within each sample was assayed by detecting the quenching of a fluorogenic substrate Dab-Gly-Pro-Leu-Gly-Met-Arg-Gly-Lys-Flu (Sigma-Aldrich) that is primarily cleaved by MMP-13, but may also be cleaved by MMP-1, -2, -3, and -9 (67). Total specific MMP activity in the culture medium was measured as the difference between a broad-spectrum MMP inhibitor, GM6001 (EMD Biosciences) and a scrambled negative control peptide (EMD Biosciences) with fluorescence measured at 485-nm excitation and 535-nm emission.

Statistical Analysis. Two-factor analysis of variance (ANOVA) with Tukey's honest significant difference post hoc test was performed to compare the different scaffold structures (variant 1 vs. variant 2) for mechanical and biochemical tests at each time point and to compare the different transgenes (eGFP vs. IL-1Ra) and media conditions (with or without IL-1) at each time point ($\alpha = 0.05$).

ACKNOWLEDGMENTS. We would like to thank Dr. James Fitzpatrick [Washington University Center for Cellular Imaging (WUCCI)] for assistance with scanning electron microscopy. This work was supported in part by NIH Grants AR55042, AR50245, AR48852, AG15768, AR48182, AG46927, and AR067467; the Collaborative Research Center; the AO Foundation (Davos, Switzerland); the Arthritis Foundation; National Science Foundation Graduate Research Fellowship 2014176256 (to A.K.R.); and the Nancy Taylor Foundation for Chronic Diseases.

1. Guilak F, Setton LA, Kraus VB (2000) Structure and function of articular cartilage. *Principles and Practice Of Orthopaedic Sports Medicine*, eds Garrett WE Jr., Speer KP, Kirkendall, DT (Lippincott Williams and Wilkins, Philadelphia), pp 53–73.
2. Heinegård D, Oldberg A (1989) Structure and biology of cartilage and bone matrix noncollagenous macromolecules. *FASEB J* 3(9):2042–2051.
3. Buckwalter JA, Martin JA, Brown TD (2006) Perspectives on chondrocyte mechanobiology and osteoarthritis. *Biorheology* 43(3-4):603–609.
4. Malchau H, Herberts P, Ahnfelt L (1993) Prognosis of total hip replacement in Sweden. Follow-up of 92,675 operations performed 1978-1990. *Acta Orthop Scand* 64(5): 497–506.
5. Robertsson O, Dunbar M, Pehrsson T, Knutson K, Lidgren L (2000) Patient satisfaction after knee arthroplasty: A report on 27,372 knees operated on between 1981 and 1995 in Sweden. *Acta Orthop Scand* 71(3):262–267.
6. Furnes O, et al. (2001) Hip disease and the prognosis of total hip replacements. A review of 53,698 primary total hip replacements reported to the Norwegian Arthroplasty Register 1987-99. *J Bone Joint Surg Br* 83(4):579–586.
7. Berry DJ, Harmsen WS, Cabanela ME, Morrey BF (2002) Twenty-five-year survivorship of two thousand consecutive primary Charnley total hip replacements: Factors affecting survivorship of acetabular and femoral components. *J Bone Joint Surg Am* 84-A(2):171–177.
8. Eskelinen A, et al. (2005) Total hip arthroplasty for primary osteoarthrosis in younger patients in the Finnish arthroplasty register. 4,661 primary replacements followed for 0-22 years. *Acta Orthop* 76(1):28–41.
9. Polkowski GG, Callaghan JJ, Mont MA, Clohisy JC (2012) Total hip arthroplasty in the very young patient. *J Am Acad Orthop Surg* 20(8):487–497.
10. McNickle AG, Provencher MT, Cole BJ (2008) Overview of existing cartilage repair technology. *Sports Med Arthrosc Rev* 16(4):196–201.
11. Woodfield TB, et al. (2009) Rapid prototyping of anatomically shaped, tissue-engineered implants for restoring congruent articulating surfaces in small joints. *Cell Prolif* 42(4):485–497.
12. Lee CH, et al. (2010) Regeneration of the articular surface of the rabbit synovial joint by cell homing: A proof of concept study. *Lancet* 376(9739):440–448.
13. Hung CT, et al. (2003) Anatomically shaped osteochondral constructs for articular cartilage repair. *J Biomech* 36(12):1853–1864.
14. Nims RJ, et al. (2015) Matrix production in large engineered cartilage constructs is enhanced by nutrient channels and excess media supply. *Tissue Eng Part C Methods* 21(7):747–757.
15. Brenner JM, et al. (2014) Implantation of scaffold-free engineered cartilage constructs in a rabbit model for chondral resurfacing. *Artif Organs* 38(2):E21–E32.
16. Bhumiratana S, et al. (2014) Large, stratified, and mechanically functional human cartilage grown in vitro by mesenchymal condensation. *Proc Natl Acad Sci USA* 111(19):6940–6945.
17. Kapoor M, Martel-Pelletier J, Lajeunesse D, Pelletier JP, Fahmi H (2011) Role of proinflammatory cytokines in the pathophysiology of osteoarthritis. *Nat Rev Rheumatol* 7(1):33–42.
18. Teunis T, et al. (2014) Soluble mediators in posttraumatic wrist and primary knee osteoarthritis. *Arch Bone Jt Surg* 2(3):146–150.
19. Sugita T, et al. (2015) Quality of life after bilateral total knee arthroplasty determined by a 3-year longitudinal evaluation using the Japanese knee osteoarthritis measure. *J Orthop Sci* 20(1):137–142.
20. Wehling N, et al. (2009) Interleukin-1beta and tumor necrosis factor alpha inhibit chondrogenesis by human mesenchymal stem cells through NF-kappaB-dependent pathways. *Arthritis Rheum* 60(3):801–812.
21. Scotti C, et al. (2012) Response of human engineered cartilage based on articular or nasal chondrocytes to interleukin-1β and low oxygen. *Tissue Eng Part A* 18(3-4): 362–372.
22. Krüger JP, et al. (2012) Chondrogenic differentiation of human subchondral progenitor cells is affected by synovial fluid from donors with osteoarthritis or rheumatoid arthritis. *J Orthop Surg* 7:10.
23. Joos H, Wildner A, Hogrefe C, Reichel H, Brenner RE (2013) Interleukin-1 beta and tumor necrosis factor alpha inhibit migration activity of chondrogenic progenitor cells from non-fibrillated osteoarthritic cartilage. *Arthritis Res Ther* 15(5):R119.
24. Heldens GT, et al. (2012) Catabolic factors and osteoarthritis-conditioned medium inhibit chondrogenesis of human mesenchymal stem cells. *Tissue Eng Part A* 18(1-2): 45–54.
25. Djouad F, et al. (2009) Transcriptomic analysis identifies Foxo3A as a novel transcription factor regulating mesenchymal stem cell chrondrogenic differentiation. *Cloning Stem Cells* 11(3):407–416.
26. Seckinger P, Dayer JM (1987) Interleukin-1 inhibitors. *Ann Inst Pasteur Immunol* 138(3):486–488.
27. Gorth DJ, et al. (2012) IL-1ra delivered from poly(lactic-co-glycolic acid) microspheres attenuates IL-1β-mediated degradation of nucleus pulposus in vitro. *Arthritis Res Ther* 14(4):R179.
28. Kraus VB, et al. (2012) Effects of intraarticular IL1-Ra for acute anterior cruciate ligament knee injury: A randomized controlled pilot trial (NCT00332254). *Osteoarthritis Cartilage* 20(4):271–278.
29. Chevalier X, et al. (2009) Intraarticular injection of anakinra in osteoarthritis of the knee: A multicenter, randomized, double-blind, placebo-controlled study. *Arthritis Rheum* 61(3):344–352.
30. Watson RS, et al. (2013) scAAV-mediated gene transfer of interleukin-1-receptor antagonist to synovium and articular cartilage in large mammalian joints. *Gene Ther* 20(6):670–677.
31. Makarov SS, et al. (1996) Suppression of experimental arthritis by gene transfer of interleukin 1 receptor antagonist cDNA. *Proc Natl Acad Sci USA* 93(1):402–406.
32. Evans CH, Ghivizzani SC, Robbins PD (2013) Arthritis gene therapy and its tortuous path into the clinic. *Transl Res* 161(4):205–216.
33. Glass KA, et al. (2014) Tissue-engineered cartilage with inducible and tunable immunomodulatory properties. *Biomaterials* 35(22):5921–5931.
34. Moutos FT, Guilak F (2010) Functional properties of cell-seeded three-dimensionally woven poly(epsilon-caprolactone) scaffolds for cartilage tissue engineering. *Tissue Eng Part A* 16(4):1291–1301.
35. Moutos FT, Freed LE, Guilak F (2007) A biomimetic three-dimensional woven composite scaffold for functional tissue engineering of cartilage. *Nat Mater* 6(2):162–167.
36. Valonen PK, et al. (2010) In vitro generation of mechanically functional cartilage grafts based on adult human stem cells and 3D-woven poly(epsilon-caprolactone) scaffolds. *Biomaterials* 31(8):2193–2200.
37. Moutos FT, Estes BT, Guilak F (2010) Multifunctional hybrid three-dimensionally woven scaffolds for cartilage tissue engineering. *Macromol Biosci* 10(11):1355–1364.
38. Ousema PH, et al. (2012) The inhibition by interleukin 1 of MSC chondrogenesis and the development of biomechanical properties in biomimetic 3D woven PCL scaffolds. *Biomaterials* 33(35):8967–8974.

39. Athanasiou KA, Agarwal A, Dzida FJ (1994) Comparative study of the intrinsic mechanical properties of the human acetabular and femoral head cartilage. *J Orthop Res* 12(3):340–349.
40. Ando W, et al. (2007) Cartilage repair using an in vitro generated scaffold-free tissue-engineered construct derived from porcine synovial mesenchymal stem cells. *Biomaterials* 28(36):5462–5470.
41. Gleghorn JP, Jones AR, Flannery CR, Bonassar LJ (2007) Boundary mode frictional properties of engineered cartilaginous tissues. *Eur Cell Mater* 14:20–28, discussion 28–29.
42. Lima EG, et al. (2006) Measuring the frictional properties of tissue-engineered cartilage constructs. *Trans Orthop Res Soc* 31:1501.
43. Morita Y, et al. (2006) Frictional properties of regenerated cartilage in vitro. *J Biomech* 39(1):103–109.
44. Plainfossé M, Hatton PV, Crawford A, Jin ZM, Fisher J (2007) Influence of the extracellular matrix on the frictional properties of tissue-engineered cartilage. *Biochem Soc Trans* 35(Pt 4):677–679.
45. Wang H, Ateshian GA (1997) The normal stress effect and equilibrium friction coefficient of articular cartilage under steady frictional shear. *J Biomech* 30(8):771–776.
46. Estes BT, Diekman BO, Gimble JM, Guilak F (2010) Isolation of adipose-derived stem cells and their induction to a chondrogenic phenotype. *Nat Protoc* 5(7):1294–1311.
47. Puetzer JL, Petitte JN, Loboa EG (2010) Comparative review of growth factors for induction of three-dimensional in vitro chondrogenesis in human mesenchymal stem cells isolated from bone marrow and adipose tissue. *Tissue Eng Part B Rev* 16(4): 435–444.
48. Wei Y, et al. (2008) A novel injectable scaffold for cartilage tissue engineering using adipose-derived adult stem cells. *J Orthop Res* 26(1):27–33.
49. Moutos FT, Guilak F (2008) Composite scaffolds for cartilage tissue engineering. *Biorheology* 45(3-4):501–512.
50. Holladay C, et al. (2009) A matrix reservoir for improved control of non-viral gene delivery. *J Control Release* 136(3):220–225.
51. Shea LD, Smiley E, Bonadio J, Mooney DJ (1999) DNA delivery from polymer matrices for tissue engineering. *Nat Biotechnol* 17(6):551–554.
52. Basile P, et al. (2008) Freeze-dried tendon allografts as tissue-engineering scaffolds for Gdf5 gene delivery. *Mol Ther* 16(3):466–473.
53. Gersbach CA, Phillips JE, García AJ (2007) Genetic engineering for skeletal regenerative medicine. *Annu Rev Biomed Eng* 9:87–119.
54. Neumann AJ, Schroeder J, Alini M, Archer CW, Stoddart MJ (2013) Enhanced adenovirus transduction of hMSCs using 3D hydrogel cell carriers. *Mol Biotechnol* 53(2): 207–216.
55. Barde I, et al. (2006) Efficient control of gene expression in the hematopoietic system using a single Tet-on inducible lentiviral vector. *Mol Ther* 13(2):382–390.
56. McNulty AL, Rothfusz NE, Leddy HA, Guilak F (2013) Synovial fluid concentrations and relative potency of interleukin-1 alpha and beta in cartilage and meniscus degradation. *J Orthop Res* 31(7):1039–1045.
57. Estes BT, Fermor B, Guilak F (2004) The influence of interleukin-1 and mechanical stimulation on human adipose-derived adult stem cells undergoing chondrogenesis. *Trans Orthop Res Soc* 29:765.
58. Gerstenfeld LC, Cullinane DM, Barnes GL, Graves DT, Einhorn TA (2003) Fracture healing as a post-natal developmental process: Molecular, spatial, and temporal aspects of its regulation. *J Cell Biochem* 88(5):873–884.
59. Brunger JM, et al. (2014) Scaffold-mediated lentiviral transduction for functional tissue engineering of cartilage. *Proc Natl Acad Sci USA* 111(9):E798–E806.
60. Serrano MC, et al. (2005) Vascular endothelial and smooth muscle cell culture on NaOH-treated poly(epsilon-caprolactone) films: A preliminary study for vascular graft development. *Macromol Biosci* 5(5):415–423.
61. Tsuji H, Ishida T, Fukuda N (2003) Surface hydrophilicity and enzymatic hydrolyzability of biodegradable polyesters: 1. Effects of alkaline treatment. *Polym Int* 52(5):843–852.
62. Salmon P, Trono D (2007) Production and titration of lentiviral vectors. *Curr Protoc Hum Genet* (Wiley, New York), pp 12.10.1–12.10.24.
63. Phillips JE, Burns KL, Le Doux JM, Guldberg RE, García AJ (2008) Engineering graded tissue interfaces. *Proc Natl Acad Sci USA* 105(34):12170–12175.
64. Elliott DM, Guilak F, Vail TP, Wang JY, Setton LA (1999) Tensile properties of articular cartilage are altered by meniscectomy in a canine model of osteoarthritis. *J Orthop Res* 17(4):503–508.
65. Mow VC, Kuei SC, Lai WM, Armstrong CG (1980) Biphasic creep and stress relaxation of articular cartilage in compression? Theory and experiments. *J Biomech Eng* 102(1): 73–84.
66. Woessner JF, Jr (1961) The determination of hydroxyproline in tissue and protein samples containing small proportions of this imino acid. *Arch Biochem Biophys* 93: 440–447.
67. Wilusz RE, Weinberg JB, Guilak F, McNulty AL (2008) Inhibition of integrative repair of the meniscus following acute exposure to interleukin-1 in vitro. *J Orthop Res* 26(4): 504–512.